Peer-reviewed version available at Minerals 2019, 9, 201; doi:10.3390/min9040201

Genesis of the Koka gold deposit in northwest Eritrea, NE Africa: Constraints from fluid inclusions, and C-H-O-S isotopes

Kai Zhao[1], Huazhou Yao[1], Jianxiong Wang[1], Ghebsha Fitwi Ghebretnsae[2], Wenshuai Xiang[1], and Yi-qu Xiong[3,4]*

[1] Wuhan Center, China Geological Survey (Central South China Innovation Center for Geosciences), Wuhan 430205, Hubei, China; 286877542@qq.com
[2] State Key Laboratory of Geological Processes and Mineral Resources, Faculty of Earth Sciences, China University of Geosciences, Wuhan 430074, P.R. China; ohghebsh@gmail.com
[3] State Key Laboratory of Geological Processes and Mineral Resources, Faculty of Earth Resources, Collaborative Innovation Center for Exploration of Strategic Mineral Resources, China University of Geosciences, Wuhan 430074, China
[4] Key Laboratory of Metallogenic Prediction of Nonferrous Metals and Geological Environment Monitoring, Ministry of Education, School of Geosciences and Info-Physics, Central South University, Changsha 410083, China
* Correspondence: xiongyiqu@126.com; Tel.: +86-18673106587

Abstract

The Koka gold deposit is located in the Elababu shear zone between the Nakfa terrane and the Adobha Abiy terrane, NW Eritrea. Based on the paragenetic study two main stages of gold mineralization were identified in the Koka gold deposit: 1) an early stage of pyrite-chalcopyrite-sphalerite-galena-gold-quartz vein; and 2) a second stage of pyrite-quartz veins. NaCl-aqueous inclusions, CO_2-rich inclusions, and three-phase CO_2-H_2O inclusions occur in the quartz veins at Koka. The ore-bearing quartz veins formed at 268°C, from NaCl-CO_2-H_2O(-CH_4) fluids averaging 5 wt% NaCl eq. The ore-forming mechanisms include fluid immiscibility during stage I, and mixing with meteoric water during stage II. Oxygen, hydrogen and carbon isotopes suggest that the ore-forming fluids originated as mixtures of metamorphic water, meteoric water and magmatic water, whereas sulfur isotope suggest an igneous origin. Features of geology and ore-forming fluid at Koka deposit are similar to those of orogenic gold deposits, suggesting the Koka deposit might be an orogenic gold deposit related to granite.

Key words: C-H-O isotopes, fluid inclusion, Koka deposit, orogenic gold deposit

1 Introduction

The Nubian Shield, locates in northeastern Africa, is an important Gondwana metallogenic domain [1,2] formed during the Neoproterozoic Pan-African orogenic cycle (ca. 900-550 Ma) [2,3]. Most of the VMS type and quartz vein-hosted gold ± sulfide deposits and occurrences of Eritrea are concentrated along NNW- and NNE- trending narrow zones in south Nubian Shield [4]. Ghebreab et al. [5] have named these zones, the Augaro-Adobha Belt (AAB) and the Asmara-Nakfa Belt (ANB). Both the world class Bisha VMS and Koka gold deposits are located in the AAB copper and gold metallogenic belt [6,7].

Koka gold deposit locates in northwest Eritrea, which has long mining history that extends

back to the Egyptian Pharaohs. However, modern mining begun in the early 20th century during the Italian colonization, until it is terminated due to the war for independence. Following the independence in 1991, several foreign mining companies from China, South Africa, India, Japan, the United Kingdom, Australia and Canada have been involved in exploring mineral potential of the country. As a result of several years of explorations, Koka gold are still with promising prospects.

Previous studies suggest the Koka deposit is a vein-type gold deposit, controlled by faults and Koka granite, and considered to be an orogenic-like gold deposit [8]. However, orogenic gold deposits are commonly unrelated to the granite [9-11], making the genesis of Koka gold deposit remain enigmatic. The key question is the metal and fluid source, and evolution history of ore-forming fluid.

Therefore, in order to understand the genesis of Koka deposit, we conducted a detailed study of deposit geology, fluid inclusions, quartz C-H-O isotope, sulfide S isotope of the Koka gold deposit, to better constrain the fluid and metal source, ore-forming fluid evolution history, and genesis.

2 Regional geology

Tectonically, Koka gold deposit is located in south Nubian Shield. The shield was formed by the collision between the East and West Gondwana upon the closure of the Mozambique Ocean during the Neoproterozoic Pan-African orogenic cycle (ca. 900-550 Ma) (Figure 1a) [3]. The prolonged tectonomagmatic evolution of ANS involves; rifting and breakup of Rodinia, formation and accretion of island-arcs, continental collision, extension and orogenic collapse [2]. Voluminous magmatic activities were also recorded associated with all the phases of the tectonic evolution. High strain NNE to NNW trending brittle-ductile shear zones conformable with major fabrics of ANS terranes are dominant in the shield [12]. Some of these shear zones containing dismembered ophiolitic suites are suggested to represent major surure zones between terranes [13]. However, others are strike-slip faults and belts of shearing and folding that have modified older sutures [14,15]. Studies have shown that the later types of shear zones are known to host numerous VMS-type polymetallic and orogenic gold deposits and occurances [15].

More than 60% of the territory of Eritrea is part of the southern Nubian Shield (Figure 1b). The geological set-up of the country is made up of three major stratigraphic successions: the basement rocks constituting the Precambrian greenstone volcano-sedimentary assemblages, which are unconformably overlain by Paleozoic and Mesozoic sedimentary and volcanic rocks, which are in turn overlain by sedimentary and volcanic rocks of Paleogene to Quaternary ages [7]. Based on lithological and structural characteristics, the Eritrean Neoproterozoic basement was divided into five tectono-stratigraphic terranes; (1) including the Barka terrane in the west, mainly composed of upper amphibolite to granulite metasedimentary and mafic gneiss complex, (2) the Hagar terranes in the north is dominated by oceanic affinity supra-subduction mafic and felsic volcanic rocks, (3) the Adobha-Abi terrane in the central and western parts is principally composed of highly deformed ophiolites and post-accretionary basinal sediments, which are imbricated by the regional shear zones, the Elababu shear zone (ESZ) in the east and the Baden shear zone (BSZ)in the west, (4) the Nakfa terrane occupying more than half of the basement complex

contains green schist facies volcano-sedimentary and syn- to post-collision granitoid rocks, (5) the easternmost Arag terrane is a narrow belt of high-grade gneiss and syn to late-tectonic granitoid rocks along the Red Sea lowlands composition [16-18].

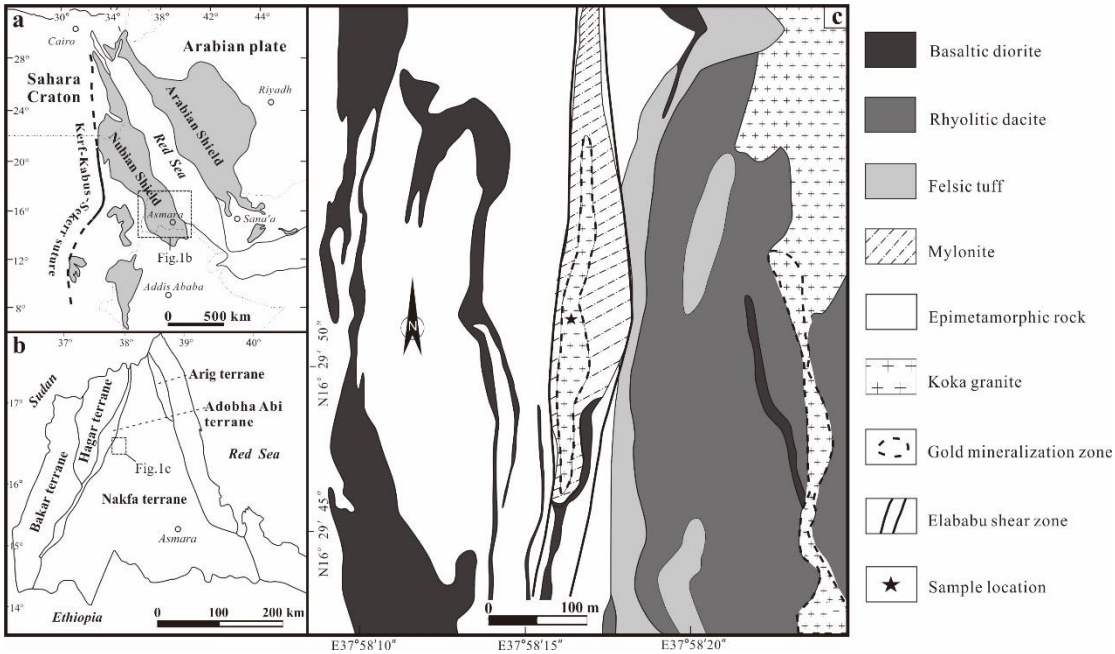

Fig.1. (**a**) Tectonic scheme of Koka deposit (after Johnson et al., 2011, [15]). (**b**) Location of Koka deposit (after Zhao et al., [19]). (**c**) Geological map of Koka gold deposit (after Dean et al., [20]).

Regional structures including; brittle-ductile shear zones and strike-slip faults, low angle thrust faults, fold structures as well as local macroscopic en-echelon quartz veins and tension gashes with a general trend of NNE to NNW are commonly developed on the Precambrian granitoid-greenstone belt. Among these, the ductile strike-slip shear zones are the most prominent tectonic structures on the region. They can be traced for several kilometers in lengths and several meters to several tens of meters in widths. The dominantly sinistral AAB and dextral ANB are the two main transpressional strike-slip shear zones, along which the important mineral deposits occur [5]. Semi-brittle shear zones developed synchronously along axial planes of isoclinal folds are also common structures on the greenschist metamorphic rocks. Syn- to late-tectonic granitoid magmatic rocks intrude along the ductile shear zones as elliptical rigid bodies [5]. These magmatic rocks are dominated by granite, granodiorite and diorite, accompanied by fine-grained rocks, dolerite and quartz porphyry [7].

3 Geology of the Koka deposit

The Koka gold mine is located in the Elababu shear zone that separates the Nakfa terrane in the east from the Adobha Abiy terrane in the west. It is hosted by a relatively fine to medium grained, gray colored, elongated nearly vertically dipping granitic body. The granitic host rock is dominated by primary minerals of plagioclase, quartz and subordinate K-feldspar with alteration products dominated by sericite, micro-granular albite and quartz. The host rock is bounded by greenschist facies metamorphic rocks, consisting intermediate to felsic volcanic and pyroclastic rocks and post-tectonic granitoids in the east part of the Nakfa

terrane and sequence of siliciclastic metasedimentary and metavolcanic rocks, including; tuffaceous greywacke, sandy mudstone, shales and mafic metabasaltic flows and associated syn-tectonic granitoid rocks in the west part of the Adobha-Abi terrane (Figure 1c). The area is dominated by the NNE shear zones, comprised of a series of asymmetric overturned isoclines folds and thrust faults, particularly prevailed on the fine grained volcanic and sedimentary rocks. The high-angle thrust faults are the main controlling structures for the ore-bearing hydrothermal activities the mine area.

In the Koka gold deposit, the mineralization was developed within the relatively competent elongated NNE trending microganitic body. Post-magmatic deformations have fractured the Koka microgranite (851.2 ±1.9Ma, [19]). These tectonic induced brittle fractures served as a pathway for the gold-bearing hydrothermal fluids and eventually became a mineralized stock works of quartz veins. The main mineralization zone can be classified into two; quartz vein type and wall-rock alteration type. The former is characterized by intense alteration and is the main mineralization zone occurring 50 to 80m from the contact of the footwall within the microgranite. This zone about 10m wide and is characterized by stock works of quartz veins with varying widths, generally no more than 2 meters. The second wall-rock alteration type mineralization is mainly developed in the contact zone between Koka microgranite and footwall metavolcano-sedimentary rocks. As of 2010, the diamond drilling had controlled constrained the Koka gold orebody over a strike length of 650m, with an average depth of more than 165m below the surface, and an average grade of about 5~6g/t, proved gold reserves are about 26.13 tons [20].

Gold is mainly formed in quartz veins in the form of native gold. Ore minerals are mainly native gold, pyrite, chalcopyrite, galena and sphalerite. Gangue minerals are mainly quartz, calcite and sericite. The types of alterations closely related to gold mineralization are silicification, sericitization, pyrite mineralization and carbonation. They are superimposed on each other in the mining area and are generally zoning. Especially silicification is consistent with the main mineralization. The sericitization and pyrite mineralization are beyond the distribution of the mineralization zone, and formed the sericite + pyrite altered halo boundary. The formation of the carbonation often occurred in the surrounding rock mainly as carbonated vein, accompanied by other alterations or separately.

Based on microscopic observations, and paragenetic study of the primary ore mineral assemblages, two main stages of mineralization are recognized in Koka gold deposit: stage I is characterized by the development of quartz-sulfide-gold veins, of which sulfides are mainly pyrite, chalcopyrite, galena and sphalerite (Figure 2a). The shape of natural gold is xenomorphic granular and it is generally distributed between pyrite and quartz (Figure 2c, e). Pyrites are mostly occurred as clusters , which are hypautomorphic-cubic crystals with large particle size changes (Figure 2d). The galena is xenomorphic granular in shape and has a distinct triangular cleavage (Figure 2f). Chalcopyrite and sphalerite are mostly showing a solid solution structure, and aggregates are also seen, occasionally a single grain (Figure 2h, g). Stage II is characterized by the development of milky white quartz veins with poor sulphide (Figure 2b). The mineral symbiosis combination is relatively simple, and only a small amount of its chalcopyrite and fine pyrite are seen.

Preprints (www.preprints.org) | NOT PEER-REVIEWED | Posted: 15 January 2019 doi:10.20944/preprints201901.0150.v1

Peer-reviewed version available at Minerals 2019, 9, 201; doi:10.3390/min9040201

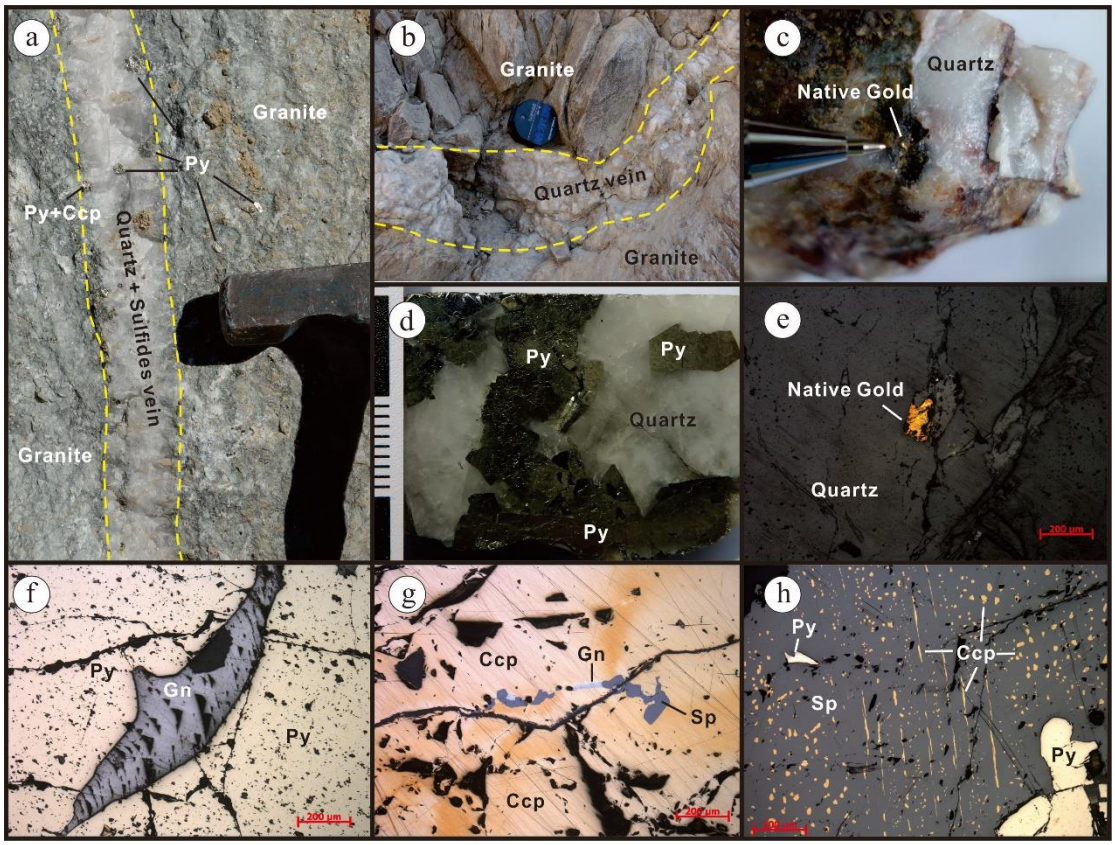

Fig. 2. Photos of orebodies, hand-specimen and minerals in microscope of Koka gold deposit. (**a**) Gold-bearing quartz veins of stage I occur in granite; (**b**) Quartz veins of stage II occur in granite; (**c**) Native gold occur in quartz veins; (**d**) Euhedral pyrite occur in quartz veins; (**e**) Native gold occur in the crack of quartz grains; (**f**) Pyrite coexists with galena; (**g**) Chalcopyrite coexists with galena and sphalerite; (**h**) Pyrite coexists with chalcopyrite and sphalerite. Abbreviations: Ccp = chalcopyrite, Gn = Galena, Py = pyrite, Sp = sphalerite.

4 Sampling and analytic method

Five ore-bearing quartz samples were collected from the Koka gold deposit, namely KO-15, KO-16, KO-17, KO-3, KO-7 and KO-14. Sampling locations are shown in Figure 1c.

Fluid inclusions

Fluid inclusion assemblages were characterized prior to selection of samples for microthermometry. Microthermometry analyses were completed in the Institute of Materials and Engineering, University of Science and Technology Beijing, using the Linkam THMSG600 heating–freezing stage (−196 to 600°C). The precision of each measurement was ±0.1°C during cooling cycles and ±1°C during heating cycles. The heating rate was held between 0.2°C/min and 10°C/min during these cycles. The temperatures of the phase transitions of the CO_2-bearing fluid inclusions and aqueous inclusions were determined at heating rates of 0.1°C/min and 0.2 to 0.5°C/min, respectively. The temperatures of the phase transitions were confirmed by the cycling technique to ensure the accuracy of the microthermometric data.

The chemical composition of the vapor phases in the fluid inclusions was determined by

Ion and gas chromatography and Raman spectroscopy at the Central South China of the Mineral Resources Supervision and Testing Center, Wuhan. Raman spectroscopy instrument was Renishaw inVia, UK. The range of spectrum range from 50cm^{-1} to 4500cm^{-1}. The operating conditions included a laser wavelength of 514.5 nm, a laser power of 30 mW. The Raman shift was calibrated using a single crystal of silicon. The cation test instrument in the liquid phase composition of the group inclusions is Hitachi Z-2300, and DIONEX ICS-3000 for ion chromatograph. GC-2014C is used for gas chromatography. The bursting temperature of the inclusions range from 100 to 550 °C, and the precision is 0.01 mg/L (0.01 μg/g).

Stable isotope analytical methods

The H–O–C isotope analyses were accomplished with a MAT253 mass spectrometer at the Analytical Laboratory of the Beijing Research Institute of Uranium Geology. The accuracy of the O isotope analysis is better than ±0.2‰, that of the H isotope analysis is better than ±2‰, and that of the C isotope analysis is typically better than ±0.1‰. The amount of O in quartz water (aquartz water) was calculated from the O isotope level of the analyzed quartz by using the fractionation equation $1000\ln\alpha_{\text{quartz water}} = (3.38 \times 10^6)T^{-2} - 3.40$, where T is the temperature in kelvins [21], and the average fluid inclusion temperature of each stage was used to calculate the $\delta^{18}O_{water}$ value.

5 Fluid inclusions

5.1 Fluid inclusion petrography

Fluid inclusions (FIs) of Koka gold deposit are found from quartz. The quartz is mainly characterized by ductile-brittle deformation. A large number of fluid inclusions, including primary, pseudosecondary and secondary fluid inclusions, were identified in two mineralization stages of quartz using detailed petrographic observations. Primary and pseudosecondary inclusions occurred in growth zoning of quartz (Figure 3e), or distributed as isolated form. The microthermometric data in this study is basically from primary and pseudosecondary inclusions. In accordance with the classification principles of Roedder [22] and Lu et al. [23], vapor-to-liquid ratios at room temperature, heating–freezing behaviors and results of laser Raman analysis were used to classify the fluid inclusions found in the Koka deposit into four types:

Type I, liquid-rich aqueous fluid inclusions (L_{H_2O}), are mainly found in the stage II, whereas rare found in stage I. Type I FIs are dominantly liquid-rich inclusions, with few pure liquid inclusions. The liquid-rich inclusions have ellipsoidal or irregular shapes with long axes of 8–16 μm and 75–95 vol% liquid phase. This type FIs are mostly primary and pseudosecondary inclusions, distributed isolated or along the crystal growth (Figure 3a, b).

Type II, CO_2-rich fluid inclusions (L_{CO_2} + V_{CO_2}), are mainly found in the early stage quartz veins. Liquid-rich CO_2 inclusions have ellipsoidal or irregular shapes with long axes of 6–16μm (Figure 3c, d, f) and 40–95 vol% liquid phase. Type II FIs were dominantly occurred as liquid phase in the room temperature (25℃), whereas few were occurred as two phases. Liquid-rich CO_2 inclusions will appear vapor in cooling process. Type II FIs commonly coexists with Type III FIs, and few coexists with Type I FIs (Figure 3d).

Type III, three-phase CO_2-rich fluid inclusions (V_{CO_2} + L_{CO_2} + L_{H_2O}) at room temperature, occurred both in the early and late stages, have ellipsoidal or irregular shapes with long axes

of 6–24μm (Figure 3a, g, h) and 20–85 vol% liquid phase.

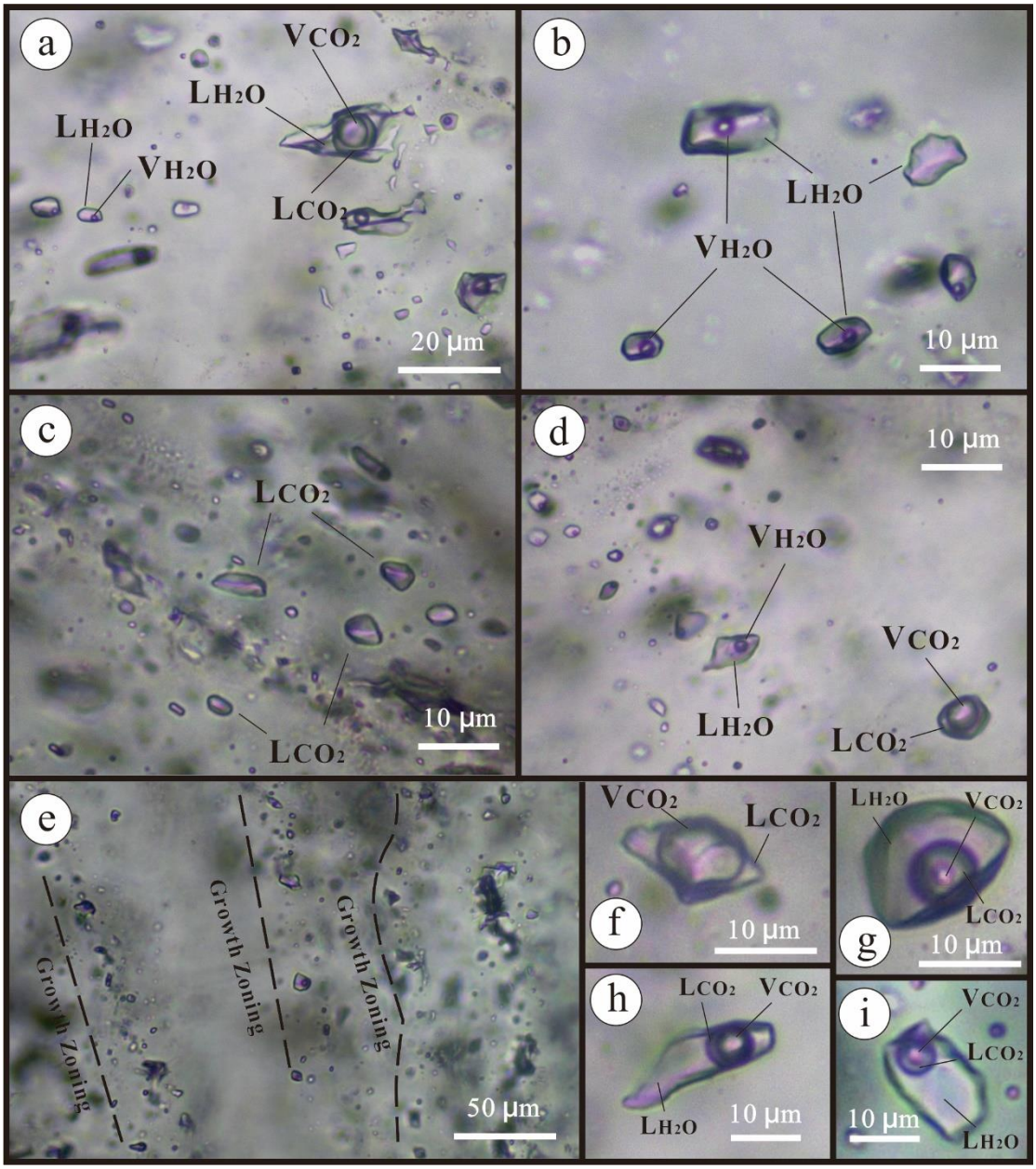

Fig. 3. (**a**) Type I FIs coexist with type III FIs in stage I veins; (**b**) Type I FIs occur in stage II veins; (**c**) Abundant Type II FIs occur in stage I veins; (**d**) Type I FIs coexist with type II FIs in stage I veins; (**e**) Primary FIs distributed along the crystal growth bands; (**f**) Type II of vapor-rich FI in stage I; (**g**) Type II of liquid-rich FI in stage I; (**h**) Type III FI in stage I; (**i**) Type III FI in stage II.

5.2 Fluid inclusion microthermometry

Five ore-bearing quartz samples from the Koka gold deposit were selected for ice melting and homogenization temperatures analysis, namely KO-15, KO-16, KO-17, KO-3, KO-7 and KO-14. One hundred and thirty-five microthermometric data of all types of fluid inclusions are listed in Table 1 and Figure 4.

Peer-reviewed version available at *Minerals* **2019**, *9*, 201; doi:10.3390/min9040201

Table 1. Summary of microthermometric data of fluid inclusions from the Koka gold deposit.

Sample No.	Stage	FI type	Size (μm)	Number	Tm,CO_2 (℃)	Tm,ice(℃)	Tm,Cl(℃)	Th,CO_2 (℃)	Th,(℃)	Salinity (wt.% NaCl)	Density (g/cm^3)
KO-15	Stage Ⅰ	Type I, minor	6~12	4		-4.3~-2.4			254~341 (V)	4.0~6.9	0.757~0.822
		Type II, abundant	8~16	9	-56.9~-58.0			-2.3~17.2			0.801~0.904
		Type III, abundant	8~16	11	-56.7~-57.9		5.7~7.8	19.2~30.1	280~356 (V)	4.3~7.9	0.576~0.793
KO-16		Type I, minor	6~12	5		-2.6~-1.9			243~288 (V)	3.2~4.3	0.711~0.831
		Type II, abundant	6~12	10	-56.7~-58.2			-4.9~18.9			0.757~0.898
		Type III, minor	6~20	14	-56.8~-58.1		5.8~7.9	19.9~29.6	235~295 (V)	4.1~7.7	0.608~0.783
KO-17		Type I, minor	6~12	6		-3.2~-1.8			223~275 (V)	3.1~5.3	0.783~0.858
		Type II, abundant	6~14	13	-56.8~-58.0			-4.7~16.4			0.812~0.901
		Type III, abundant	10~24	14	-56.6~-58.0		5.3~8.0	10.6~29.4	238~305 (V)	3.3~8.5	0.613~0.862
KO-3		Type I, abundant	8~16	6		-2.6~-1.5			221~288 (V)	2.6~4.3	0.765~0.872
		Type III, abundant	8~20	11	-57.0~-57.9		6.2~8.2	19.7~29.7	228~295 (V)	3.5~7.1	0.613~0.787
KO-7	Stage Ⅱ	Type I, abundant	8~12	6		-2.8~-1.3			212~280 (V)	2.2~4.7	0.763~0.871
		Type III, abundant	8~24	11	-56.9~-57.4		6.6~8.5	18.5~29.7	232~318 (V)	3.0~7.5	0.597~0.793
KO-14		Type I, minor	8~14	5		-2.6~-0.9			235~267 (V)	2.2~4.3	0.786~0.842
		Type III, abundant	10~22	10	-56.7~-57.3		5.6~8.0	18.2~25.7	259~309 (V)	3.9~8.0	0.672~0.701

Preprints (www.preprints.org) | NOT PEER-REVIEWED | Posted: 15 January 2019 doi:10.20944/preprints201901.0150.v1

Peer-reviewed version available at Minerals 2019, 9, 201; doi:10.3390/min9040201

(1) Stage I

The fluid inclusions in stages I included types I, II, and III, FIs. Type I FIs homogenized to the liquid phase at temperatures ranging from 254 ℃ to 341 ℃, predominantly at 260–280 ℃. Their ice melting temperatures ranged from –4.3 ℃ to –1.8 ℃, corresponding to salinities of 3.1–6.9 wt% NaCl eqv, with most around 3–4 wt% NaCleqv. Type II fluid inclusions showed the CO_2 phase melting temperatures ranged from –56.7 ℃ to –58.2 ℃, with peak at –57℃, and the temperatures of homogenization to the liquid phase of –4.9 ℃ to 18.9 ℃. Type III (CO_2-rich) inclusions formed solid CO_2 upon cooling. The solid CO_2 melted at temperatures between –56.6 ℃ and –58.1 ℃, lower than the triple point temperature of pure CO_2 (–56.6 ℃). The CO_2-clathrate melting temperatures varied from 5.3℃ to 8.0 ℃, corresponding to salinities of 3.3–8.5wt%NaCl eqv, with most around 6–7 wt% NaCl eqv. Vapor- and liquid-CO_2 homogenized to the vapor phase at temperatures between 10.6 ℃ and 30.1 ℃, higher than the type II FIs in stage I (Figure 5). The total homogenization temperatures of type III inclusions ranged from 235 ℃ to 356 ℃, with most around 280–300 ℃.

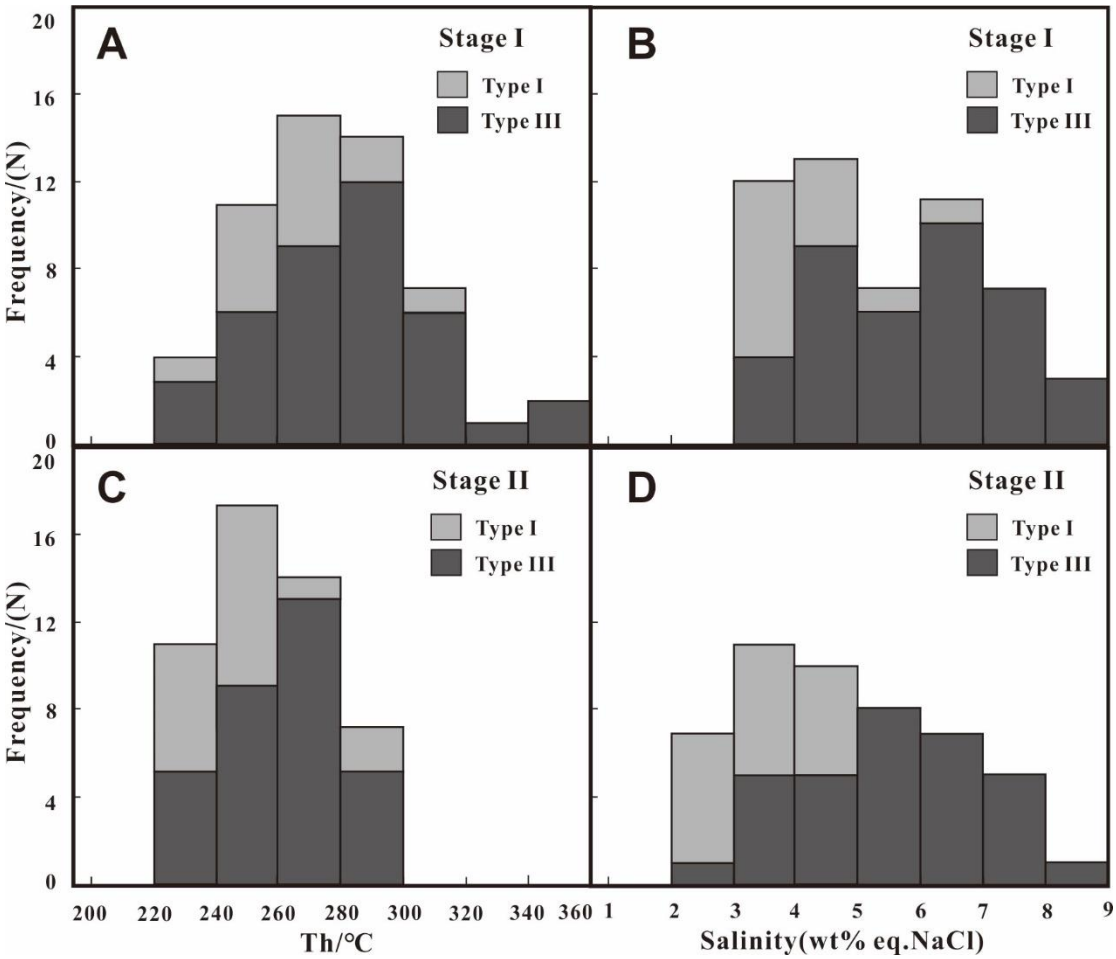

Fig. 4. (**A, C**). Homogenization temperature of different stages of Koka gold deposit; (**B, D**). Salinity of different stages of Koka gold deposit.

(2) Stage II

The fluid inclusions in stages II included types I, III, and rare type II FIs, and the

Preprints (www.preprints.org) | NOT PEER-REVIEWED | Posted: 15 January 2019 doi:10.20944/preprints201901.0150.v1

Peer-reviewed version available at Minerals 2019, 9, 201; doi:10.3390/min9040201

inclusions of type III are commonly vapor-rich (V/ (V + L) > 40%). The FIs of type I are dominantly liquid-rich, and homogenized to the liquid phase at temperatures varying from 212 ℃ to 288 ℃, predominantly at 260–280 ℃. Their ice melting temperatures ranged from –2.8 ℃ to –0.9 ℃, corresponding to salinities of 2.2–4.7 wt% NaCl eqv, with most around 3–4 wt% NaCleqv. Type II fluid inclusions showed the CO_2 phase melting temperatures ranged from –56.9 ℃ to –57.9 ℃, and the temperatures of homogenization to the liquid phase of 6.8 ℃ to 17.3 ℃. The solid CO_2 of type III inclusions melted at temperatures between –56.9 ℃ and –57.9 ℃, and the CO_2-clathrate melting temperatures varied from 6.2℃ to 8.5 ℃, corresponding to salinities of 3.0–8.0 wt% NaCl eqv, with most around 5–7 wt% NaCl eqv. Vapor- and liquid-CO_2 homogenized to the liquid phase at temperatures between 18.5 ℃ and 29.7 ℃, and the total homogenization temperatures of type III inclusions ranged from 232 ℃ to 318 ℃, with most around 260–280 ℃.

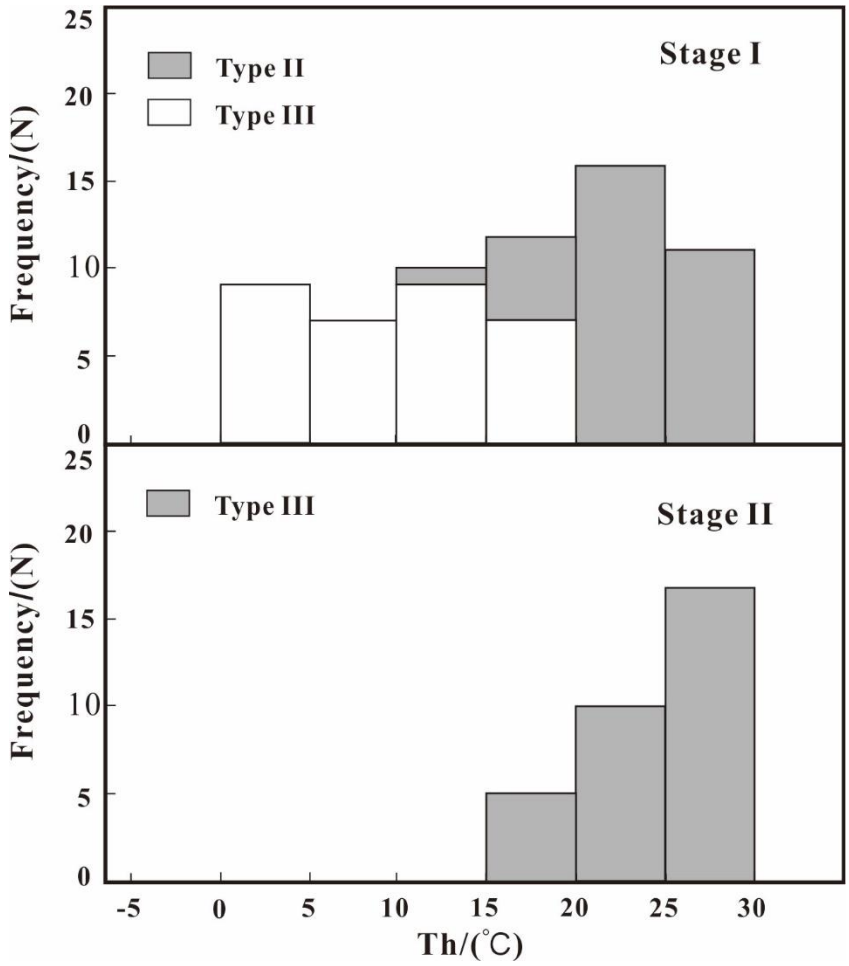

Fig. 5. Homogenization temperature of vapor phase CO_2 in different stages of Koka gold deposit.

5.3 Laser Raman spectroscopy

Selected samples based on fluid inclusion petrology of two stages were examined by Laser Raman micro spectroscopy. The results show that composition of FIs in type I is relatively simple, dominated by H_2O (Figure 6d). The composition of type II FIs is basically pure CO_2 (Figure 6c) . The inclusion gas of type III is dominated by CO_2 and H_2O, and the

aqueous phase also contained some CO_2 (Figure 6a, b).

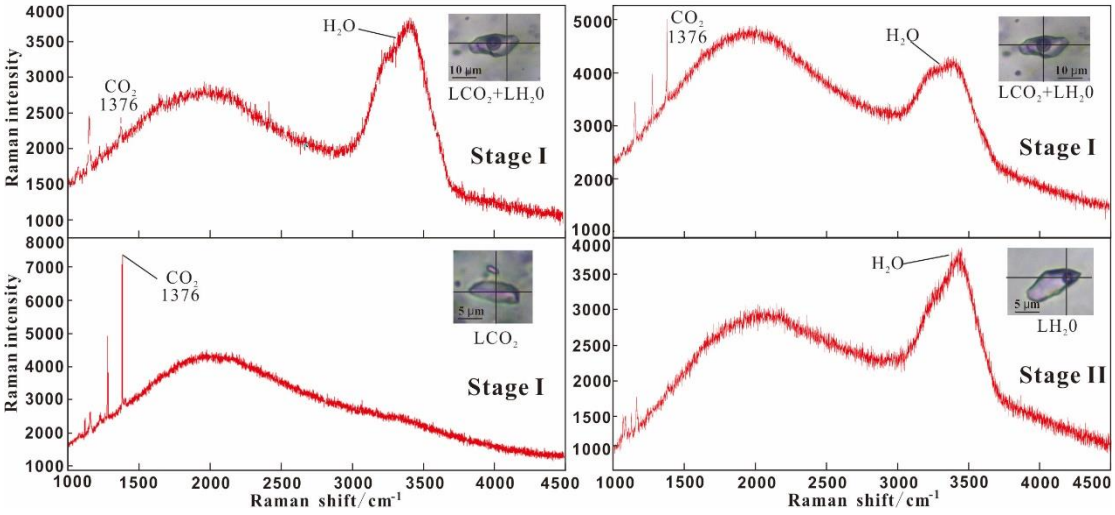

Fig. 6. Raman spectra of the fluid inclusion of Koka gold deposit.

5.4 Ion and gas chromatography

The result of compositions of fluid inclusions cluster in quartz based on ion and gas chromatography shows that the CO_2 and H_2O are the dominant gaseous ingredient, and rare CH_4 (Table 2). The average mole% of H_2O and CO_2 of stage I are 0.535 and 0.465, respectively, whereas the average mole% of H_2O increased to 0.753, and the average mole% of and CO_2 reduced to 0.245 in stage II. Only 0.11 mole% of CH_4 was detected in sample KO-16 of stage I.

The result of ion chromatography shows that the Na^+ is the dominant cation in both stages, with minor K^+ and Ca^+, and the ratio of Na^+/K^+ ranges from 20.13 to 26.33, and 12.75 to 17.15, respectively. The anion of the two stages is mainly Cl^-, with minor SO_4^{2-}, and the ratio of Cl^-/SO_4^{2-} ranges from 11.52 to 17.42, and 19.24 to 31.26, respectively. Moreover, the average content of Na^+ and Cl^- in stage I is 5.40 mg/L and 6.96 mg/L, respectively. Compared with stage I, the average contents of Na^+ and Cl^- in stage II are 9.64 mg/L and 12.63 mg/L, respectively, higher than stage I.

Table 2. Results of ion and gas chromatography of fluid inclusions from the Koka gold deposit.

Sample No	Stage	H_2O (mol%)	CO_2 (mol%)	CO (mol%)	CH_4 (mol%)	H_2 (mol%)	K^+ (ppm)	Na^+ (ppm)	Ca^{2+} (ppm)	Mg^{2+} (ppm)	Li^+ (ppm)	F^- (ppm)	Cl^- (ppm)	SO_4^{2-} (ppm)	Br^- (ppm)
KO-15	Stage Ⅰ	0.595	0.405	＜0.01	＜0.01	＜0.01	0.18	4.74	0.09	0.02	＜0.01	＜0.01	5.99	0.52	＜0.01
KO-16		0.526	0.474	＜0.01	＜0.01	＜0.01	0.31	6.24	0.07	＜0.01	＜0.01	＜0.01	8.36	0.48	＜0.01
KO-17		0.484	0.516	＜0.01	＜0.01	＜0.01	＜0.01	5.22	0.06	＜0.01	＜0.01	＜0.01	6.52	0.56	＜0.01
KO-3	Stage Ⅱ	0.741	0.259	＜0.01	＜0.01	＜0.01	0.47	8.06	0.08	＜0.01	＜0.01	＜0.01	9.62	0.50	＜0.01
KO-7		0.765	0.235	＜0.01	＜0.01	＜0.01	0.88	11.22	0.10	0.02	＜0.01	＜0.01	15.63	0.50	＜0.01

Preprints (www.preprints.org) | NOT PEER-REVIEWED | Posted: 15 January 2019 doi:10.20944/preprints201901.0150.v1

Peer-reviewed version available at Minerals 2019, 9, 201; doi:10.3390/min9040201

6 C-H-O-S Isotopes

The carbon and oxygen isotopic data are listed in Table 3 and plotted in Figure 7. Three quartz samples from the early stage give the $\delta^{13}C$ value ranges from −5.5‰ to −5.0‰, and the $\delta^{18}O$ value ranges from +9.0‰ to +9.7‰. The $\delta^{13}C$ and $\delta^{18}O$ values of two quartz samples from the late stage fall within a range of −4.4‰ and +10.1‰ to +10.8‰, respectively.

Table 3. Oxygen, hydrogen and carbon isotopic compositions of quartz from Koka gold deposit.

Sample NO.	Stage	Mineral	δDsmow (‰)	$\delta^{18}O_{smow}$ (‰)	$\delta^{18}OH_2O$ (‰)	$\delta^{13}C_{v\text{-}PDB}$ (‰)	Temperature(℃)
KO-15	Stage Ⅰ	Quartz	-52.5	9.7	2.4	-5.0	290
KO-16		Quartz	-57.0	9.0	1.7	-5.4	290
KO-17		Quartz	-50.1	9.5	2.2	-5.5	290
KO-3	Stage Ⅱ	Quartz	-53.1	10.8	2.7	-4.4	270
KO-7		Quartz	-54.1	10.1	2.0	-4.4	270

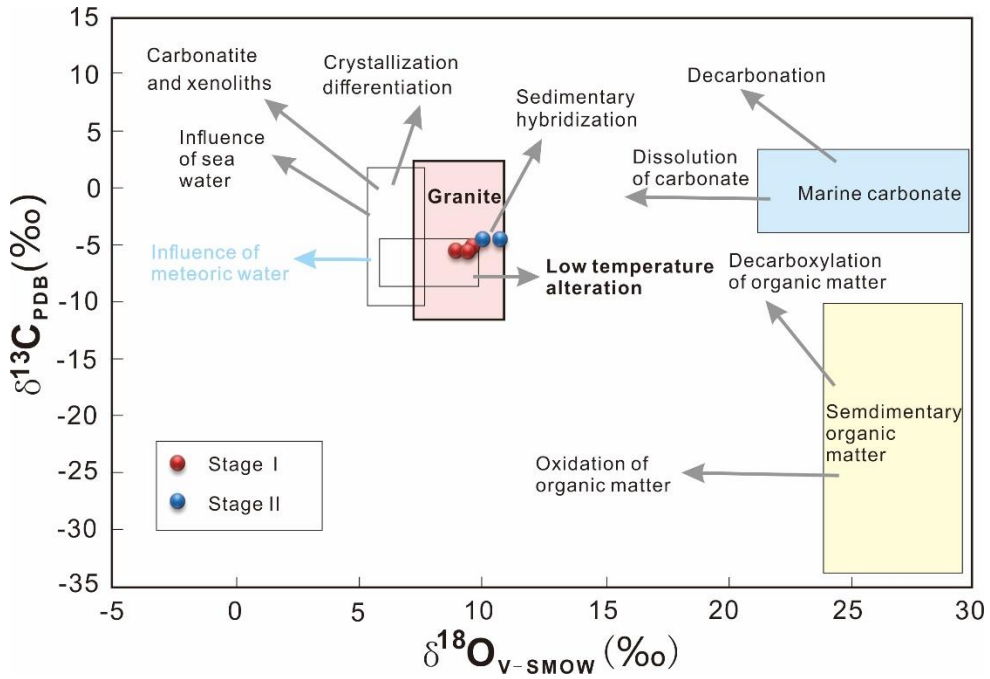

Fig. 7. Calculated $\delta^{13}C$ and $\delta^{18}O$ values of fluids at Koka (after Chen et al., 2012, [40]).

The oxygen and hydrogen isotopic data are listed in Table 3 and plotted in Figure 8. The measured $\delta^{18}O$values of five quartz samples in two stages range from+8.0 to+8.8‰. The $\delta^{18}O$ values of hydrothermal fluids were calculated using the equation of Clayton et al. [21], $1000\ln a_{quartz-water} = 3.38 \times 10^6 \times T^{-2} - 3.40$, together with the measured $\delta^{18}O_{quartz}$ values and the correspondingly average homogenization temperatures of the FIs in the same stage of the same sample (Table 3). As a result, the $\delta^{18}O_{H2O}$ values from the early stage and the late stage are +1.7‰ to +2.4‰, and 2.0‰ to +2.7‰, respectively. All samples selected for $\delta^{18}O$ analysis were also analyzed for their hydrogen isotopic composition. The δD_{H2O} values of the quartz

Preprints (www.preprints.org) | NOT PEER-REVIEWED | Posted: 15 January 2019 doi:10.20944/preprints201901.0150.v1

Peer-reviewed version available at Minerals 2019, 9, 201; doi:10.3390/min9040201

samples in the early stage and the late stage are −57.0‰ to −50.1‰, and −54.1‰ to −53.1‰, respectively.

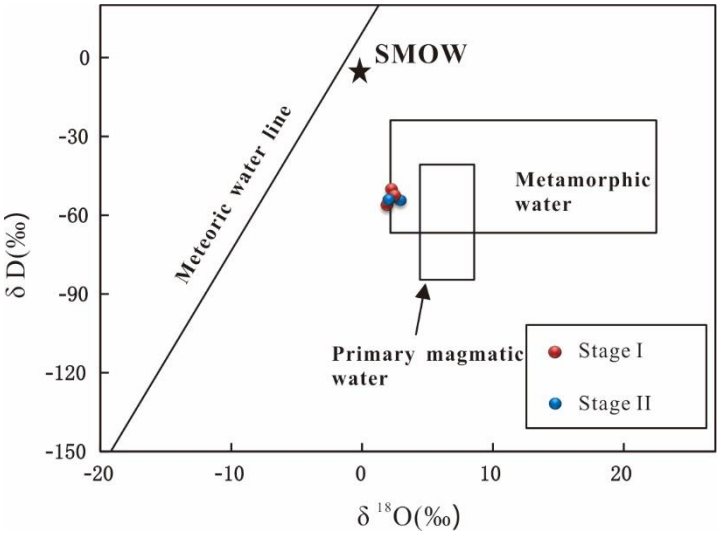

Fig. 8. $\delta^{18}O$ and δD values of the ore fluids at Koka deposit. Metamorphic water field, primary magmatic water field, and meteoric water line are from Taylor (1974), [35].

The sulfur isotopic data are shown in Table 4 and plotted in Figure 9. The $\delta^{34}S$ values of ten pyrite samples from the Koka gold deposit range from −0.1‰ to +2.7‰, with an average of +1.6‰, the $\delta^{34}S$ value of one chalcopyrite, one galena and one sphalerite samples are +1.3‰, −1.3‰, and +1.2‰, respectively. Therefore, sulfur isotopic compositions in the Koka gold deposit show a relatively narrow range (−1.3 to +2.7‰, around zero), indicating a homogenous sulfur source.

Table 4. Sulfur isotopic compositions of sulfides from Koka gold deposit.

Sample No.	Stage	Mineral	$\delta^{34}S_{CDT}$ (‰)
KO-11	Stage Ⅰ	Pyrite	1.7
KO-11		Pyrite	-0.1
KO-15		Pyrite	1.3
KO-16		Pyrite	1.4
KO-17		Pyrite	1.6
KO-17		Pyrite	1.6
KO-17		Chalcopyrite	1.3
KO-17		Galena	-1.3
KO-17		Sphalerite	1.2
KO-3	Stage Ⅱ	Pyrite	1.9
KO-3		Pyrite	1.9
KO-7		Pyrite	2.7
KO-14		Pyrite	1.8

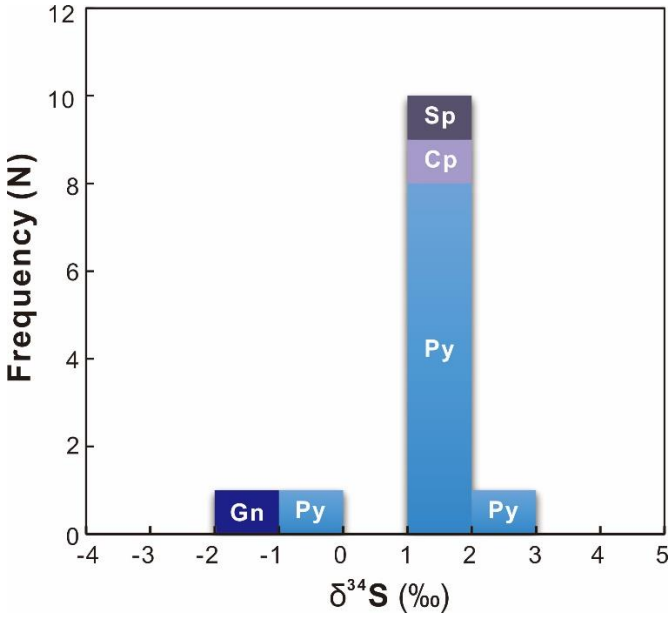

Fig. 9. Histograms of $\delta^{34}S$ values of sulfide for the Koka deposit.

7 Discussion

7.1 Nature and evolution of ore-forming fluid

CO_2-bearing FIs are the most abundant occurred in the Koka gold deposit, with moderate liquid-rich aqueous FIs. Generally, the results of fluid inclusion petrography, microthermometry and laser Raman micro-spectroscopy shows that the ore-forming fluid of the KoKa gold deposit is a medium- to low-temperature and low-salinity CO_2-NaCl-H_2O system.

1) Stage I

The ore-forming fluid of this stage is medium-temperature, low-salinity NaCl-H_2O-CO_2(-CH_4) fluid (CH_4 was detected via gas chromatography). Majority of CO_2 and CH_4 are likely from the metamorphic strata [24,25,10]. Fluid immiscibility is one of the dominant ore-forming mechanisms in gold deposits [26-28]. The common coexistence of type I and II FIs during stage I suggests that they were entrapped simultaneously, and homogenized in different ways, which suggests that fluid immiscibility occurred prior to their entrapment [29]. The plot of salinity vs. the homogenization temperatures (Figure 10) indicates that the ore-forming fluid underwent a fluid immiscibility process during stage I at Xiangdong (three-phase CO_2-rich inclusions commonly coexist with two-phase aqueous inclusions in quartz, with similar homogenization temperatures, [22]), which is likely due to the temperature and pressure decrease as the ore-forming fluid ascended, leading to escape of CO_2 from the fluid.

Preprints (www.preprints.org) | NOT PEER-REVIEWED | Posted: 15 January 2019 doi:10.20944/preprints201901.0150.v1

Peer-reviewed version available at Minerals 2019, 9, 201; doi:10.3390/min9040201

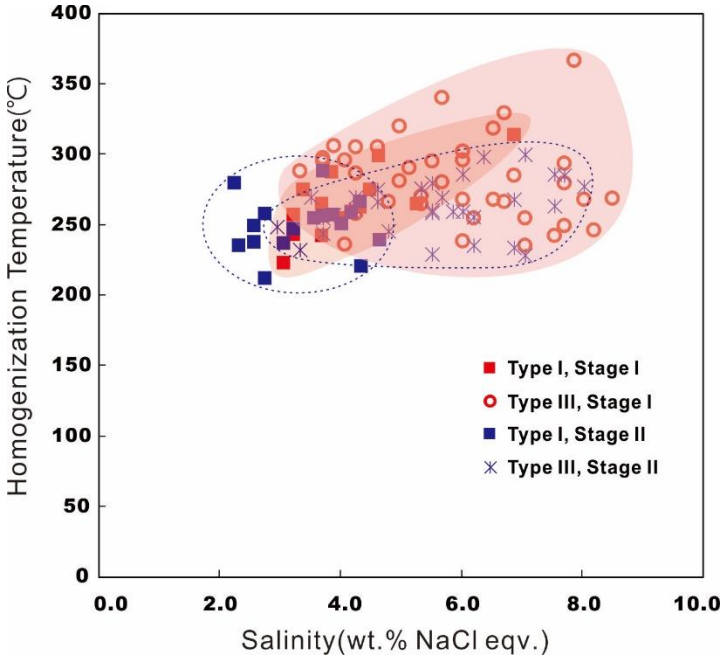

Fig. 10. Plot of salinity vs. homogeneous temperature for fluid inclusions of different stages from the Koka deposit.

Moreover, varying degrees of CH_4 involvement in the fluid system were detected in the stage I FIs, and CH_4 may lead to fluid immiscibility of the NaCl–H_2O–CO_2 system in the depth [30].

We calculated the densities via Flincor software [31] of the type I (salinity<5 wt% NaCleqv) and the type II (CO_2-rich) inclusions in stage I at 0.711–0.858 g/cm^3 and 0.757–0.904 g/cm^3, respectively, and then estimated the pressure at 176 MPa (range from 73 to 278 MPa, Figure 11 [32,33]), which is similar with the estimated pressure 178 MPa (range from 105 to 250 MPa, Figure 12) using the method of Van den Kerhof and Thiéry [34]. Hence ~176 MPa can represent the actual trapping pressure of stage I, corresponding to depth of 6.7 km (lithostatic pressure; rock density of 2.7 g/cm^3).

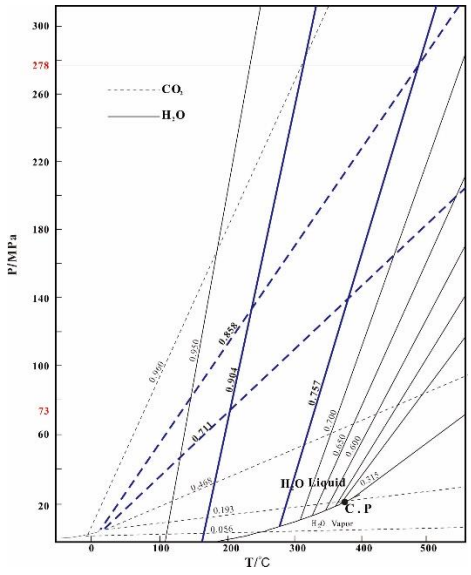

Preprints (www.preprints.org) | NOT PEER-REVIEWED | Posted: 15 January 2019 doi:10.20944/preprints201901.0150.v1

Peer-reviewed version available at Minerals 2019, 9, 201; doi:10.3390/min9040201

Fig. 11. Pressure estimations for primary fluid inclusions of Koka deposit (after Roedder and Bodnar ,1980, [32]).

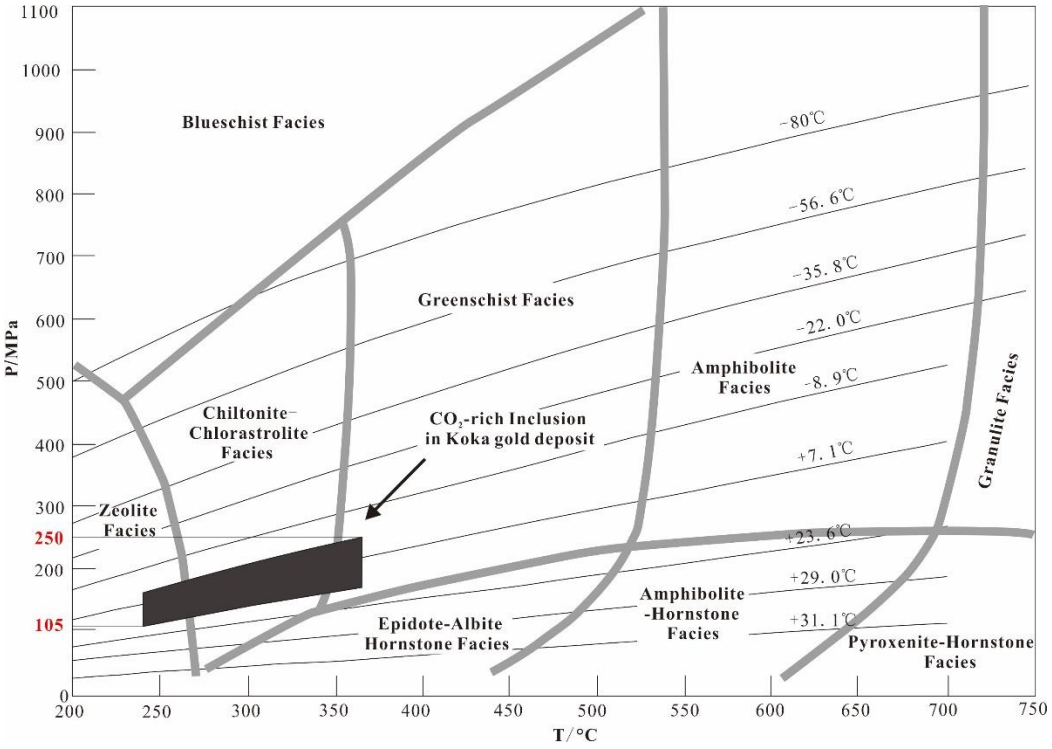

Fig. 12. Pressure estimations for primary fluid inclusions of Koka deposit (after Van den Kerhof and Thiéry 2001, [34]).

2) Stage II

The occurrence and composition of different FIs types suggest the ore-forming fluid from stage II is a medium-temperature, low-salinity NaCl-H_2O-CO_2 fluid. The temperature of the ore-forming fluid decreased from stage I to II, probably due to the progressive cooling of the fluid system or/and mixing with relatively low-T fluid, whereas the meteoric water mixing is supported by the results of hydrogen and oxygen isotopes. In addition, water content increased in fluid of stage II, suggesting a water mixing. Salinity from stage I to II changed slightly likely due to the precipitation of metal elements in stage II.

7.2 Source of ore-forming fluids and metal

Most of the δD_{fluid} values (–57.0 to –50.1‰) and the $\delta^{18}O_{H2O}$ values (+1.7 to +2.7‰) of the ore quartz in the Koka gold deposit fall within the ranges of the isotopic compositions of metamorphic water [35], and near the primitive magmatic water field. In addition, two of the data drift toward the meteoric water line (Figure 8). The H–O data suggests that these ore-forming fluids were derived from metamorphic water and magmatic water and meteoric water could mix within the ore-forming fluids.

The $\delta^{13}C$ values of quartz samples range from−5.5 to−4.4‰, which are higher than those of the organic matter (averaging −25‰, [36]), CO_2 dissolved in water (−9 to −20‰, [37]), atmospheric CO_2 (~ −8‰, [38] or −7 to −11‰, [37]), and crust (−7‰, [39]), and lower than the

marine carbonates (~0‰, [36]), but consistent with the C isotopic compositions of igneous/magma systems (−3 to −30‰, [37]; mantle (−5 to −7‰, [36]). In the $\delta^{13}C$ vs. $\delta^{18}O$ diagram, all the quartz samples plot within the granite box field (Figure 7), indicating that carbon in the early ore-forming fluids was likely to be provided by magmatic water. Moreover, the late stage quartz samples show obvious trend of influence by low temperature alteration, which suggests a temperature cooling in the late ore-forming system. This interpretation is consistent well with the results of fluid inclusion microthermometry.

The $\delta^{34}S$ values of sulfides in the Koka gold deposit exhibit a narrow range values that are close to 0‰(−1.3 to +2.7‰, Figure 9), which suggests that the sulfides that precipitated from the fluid system originated from a single sulfur source that primarily comprised deep-seated magma ($\delta^{34}S$ = 0 ± 3‰, [41,42]). Moreover, the $\delta^{34}S$ values exhibited a trend of $\delta^{34}S_{pyrite}>\delta^{34}S_{sphalerite}>\delta^{34}S_{galena}$, which is consistent with the crystallization sequence of minerals in a hydrothermal system under the conditions of sulfur isotopic fractionation equilibrium. These data suggest that the hydrothermal system reached a state of sulfur isotopic fractionation equilibrium before its ore minerals were precipitated [43-45], suggesting that these ore-forming materials were predominantly sourced from magma.

7.3 Genetic model for ore deposition

The continent collision of the East and West Gondwana caused the re-construction of the regional juvenile crust and lithosphere, and the formation of EAOB during Neoproterozoic (~650 Ma). Most of the juvenile crust were conjoined along the arc-arc suture, and the subsequent orogeny lasted nearly 100 Ma [15]. Due to the rapid convergence between the east Gondwana and west Gondwana, the Eritrea region in the southern part of the EAOB was experienced regional metamorphism [46].

^{40}Ar-^{39}Ar ages of sericite in gold-bearing quartz veins of Koka deposit is 600-580 Ma (unpub. data), suggesting the Koka deposit is likely formed in Neoproterozoic. Moreover, several gold deposits in Nubian Shield were reported to formed at this period, such as Sukhaybarat [47], An Najadi [48], Ad Duwayhi [49] and Lega-Dembi [50]. Regionally, Post orogenic a-type granite was formed after 610 Ma [15], combined with the formation age of Kyanite schist (U-Pb age of monazite, 593±5Ma, [51]), suggesting the time interval of 600-580 Ma is in the transition environment from crust compression to extension during the collision and accompanied with regional metamorphism.

The characteristics of geotectonic environment, occurrence of orebodies, mineral assemblages, and ore-forming fluid of Koka gold deposit are similar to the features of orogenic gold deposit [28,52,53], whereas carbon and sulfur isotopes suggests igneous origin. Hence, the Koka gold deposit could be an orogenic gold deposit related to magmatism. The detailed ore-forming process is described as:

After the solidification of Koka granite, multi-fractures were existed in the granite and became a relatively low-pressure zone in the district. Ore-bearing fluid, which was derived from metamorphic strata and containing abundant CO_2 in in high-pressure conditions, was driven by regional thermodynamic processes to flow into the fault system of Koka granite. The temperature and pressure decrease as the ore-forming fluid rises during stage I, which leads to CO_2 separating from the fluid and accompanied with fluid immiscibility, leading to the dissolution of the Au-bearing complexes and a pH changing of the residual fluid. And

then ore-forming ions, such as Au^{+}, Fe^{2+}, Cu^{2+}, Pb^{2+}, Zn^{2+}, and S^{2-} were precipitated at locations with advantageous structural conditions. During stage II, meteoric water mixed in and cooling the fluid system, metal cations, such as Fe^{2+}, S^{2-} remained in the fluid were deposited in the structural fractures and micro-fractures of the existing veins.

Conclusion

1) The ore-forming fluid of the KoKa gold deposit is a medium- to low-temperature and low-salinity CO_2-NaCl-H_2O system, and ore-forming mechanisms include fluid immiscibility during an early stage and fluid mixing with meteoric water in subsequent stages at lower temperature. Using two methods to estimate a similar pressure at ~176 MPa, corresponding to depth of 6.7 km.

2) C-H-O isotopic compositions indicate that the ore-forming fluids of the Koka deposit could have originated from metamorphic strata and were mixed with meteoric water, with considerable magmatic contribution. S isotopic result suggest the metals were derived from magma.

3) Features of geology and ore-forming fluid at Koka gold deposit are similar to those of orogenic gold deposits. Hence the Koka deposit might be an orogenic gold deposit related to granite.

Author Contributions: K. Zhao, H.Z. Yao, J.X. Wang, and Y.Q. Xiong conceived and designed the experiments; G.F.G., and W.X. performed the experiments; all authors wrote the paper.

Funding: This research was funded by [China Geological Survey, Mineral resources assessment of Egypt and adjacent areas] grant number [DD20160109], [the National Natural Science Foundation of China Project] grant number [41803044] and [the Construction Project of National Technical Standard System of Mineral Resources and Reserves] grant number [CB2017-4-10; 2017TP1029].

Acknowledgments: This work was supported by the China Geological Survey, Mineral resources assessment of Egypt and adjacent areas (DD20160109), Evaluation of large copper and gold resource bases in North Africa Project, and the National Natural Science Foundation of China Project (grant number 41803044).

Conflicts of Interest: The authors declare no conflict of interest.

References

1. Kröner, A.; Eyal, M.; Eyal, Y. Early Pan-African evolution of the basement around Elat, Israel and the Sinai Peninsula revealed by single-zircon evaporation dating and implication for crustal accretion rates. *Geology*. **1990**, 18, 545–548.
2. Stern, R.J. Neoproterozoic (900–550 ma) arc assembly and continental collision in the east Africa orogen : implications for the consolidation of Gondwanaland. *Annual Review of Earth & Planetary Sciences*. **1994**, 22, 319–351.
3. Stern, R.J. Neoproterozoic crustal growth: the solid Earth system during a critical episode of Earth history. *Gondwana Research*. **2008**, 14, 33–50.
4. Johnson, P.R.; Zoheir, B.A.; Ghebreab, W.; Stern, R.J.; Barrie, C.T.; Hamer, R.D. Gold-bearing volcanogenic massive sulfides and orogenic-gold deposits in the Nubian Shield. *South African Journal of Geology*. **2017**, 120, 6376.
5. Ghebreab, W.; Greiling, R.O.; Solomon, S. Structural setting of Neoproterozoic mineralization, Asmara district, Eritrea. *Journal of African Earth Sciences*. **2009**, 55, 219–235.

6. Barrie, C.T.; Nielsen, F.W.; Aussant, C.H. The Bisha volcanic-associated massive sulfide deposit, western Nakfa terrane, Eritrea. *Economic Geology*. **2007**, 102, 717–738.
7. Zhao, X.Z.; Duan, H.C.; Wang, F.X. General characteristics of geology and mineral resources in Eritrea and exploration progress. *Mineral Exploration*. **2012**, 5, 707–714. (in Chinese)
8. Xiang, P.; Wang, J.X. Ore geology character and type of Koka gold deposit, Eritrea. *Acta Mineralogica Sinica*. **2013**, s2, 1067–1068. (in Chinese)
9. Goldfarb, R.J.; Groves, D.I.; GardollS. Orogenic gold and geologic time: A global synthesis. *Ore Geology Reviews*. **2001**, 18, 12–75.
10. Groves, D.I.; Goldfarb, R.J.; Robert, F. Gold deposits in metamorphic belts: overview of current understanding, outstanding problems, future research, and exploration significance. *Economic Geology*. **2003**, 98, 1–29.
11. Goldfarb, R.J.; Groves, D.I. Orogenic gold: Common or evolving fluid and metal sources through time. *Litho*. **2015**, 233, 2–26.
12. Abdelsalam, M.; Stern, R. Sutures and shear zones in the Arabian-Nubian Shield. *Journal of African Earth Sciences*. **1996**, 23, 289–310.
13. Stern, R.J.; Johnson, P.R.; Kröner, A.; Yibas, B. Neoproterozoic ophiolites of the Arabian-Nubian shield. *Developments in Precambrian Geology*. **2004**, 13, 95–128.
14. Johnson, P.R.; Woldehaimanot, B. Development of the Arabian–Nubian shield: perspectives on accretion and deformation in the northern East African Orogen and the assembly of Gondwana. *London, Special Publication*. **2003**, pp, 290–325.
15. Johnson, P.R.; Andresen, A.; Collins, A.S.; Fowler, A.R.; Fritz, H.; Ghebreab, W.; Kusky, T.; Stern, R.J. Late Cryogenian–Ediacaran history of the Arabian–Nubian shield: A review of depositional, plutonic, structural, and tectonic events in the closing stages of the northern East African Orogen. *Journal of African Earth Sciences*. **2011**, 61, 167–232.
16. Drury, S.A.; Berhe, S.M. Accretion tectonics in Northern Eritrea revealed by remotely sensed imagery. *Geological Magazine*. **1993**, 130, 177–190.
17. Teklay, M. *Petrology, geochemistry and geochronology of Neoproterozoic magmatic arc rocks from Eritrea: implications for crustal evolution in the southern Nubian Shield*. Department of Mines-Ministry of Energy Mines and Water Resources-State of Eritrea. **1997**, 1, 1–125.
18. Drury, S.A.; De Souza Filho, C.R. Neoproterozoic terrane assemblages in Eritrea: review and prospects. *J. Afr. Earth Sci*. **1998**, 27, 331–348.
19. Zhao, K.; Yao, H.Z.; Wang, J.X.; Ghebsha, F.G.; Xiang, W.S.; Yang, Z. Zircon U-Pb geochronology and geochemistry of Koka granite and its geological significances, Eritrea. *Earth Science* (in press). (in Chinese)
20. Dean, C.; David, L.; David, G. *Technical report on the Koka gold deposit, Eritea*. Chalice Gold Mine Limied. **2010**, pp, 1–111.
21. Clayton, J.; Tretiak, D.N. Amine-citrate buffers for pH control in starch gel electrophoresis. *Journal of the Fisheries Board of Canada*. **1972**, 29, 1169–1172.
22. Roedder, E. Fluid inclusions. Review in mineralogy 12, Mineralogical Society of America. *Michigan: Book Crafters, Inc*. **1984**, pp, 1–644.
23. Lu, H.Z.; Fan, H.R.; Ni, P.; Ou, G.X.; Shen, K.; Zhang, W.H. *Fluid inclusions*. Beijing. Science Press. **2004**, pp, 406–419. (in Chinese)
24. Yang, L.Q.; Deng, J.; Guo, L.N.; Wang, Z.L.; Li, X.Z.; Li, J.L. Origin and evolution of ore fluid, and gold-deposition processes at the giant Taishang gold deposit, Jiaodong Peninsula, eastern China. *Ore Geology Reviews*. **2016a**, 72, 585–602.
25. Yang, L.Q.; Guo, L.N.; Wang, Z.L.; Zhao, R.X.; Song, M.C.; Zheng, X.L. Timing and mechanism of gold mineralization at the Wang'ershan gold deposit, Jiaodong Peninsula, eastern China. *Ore Geology Reviews*. **2017**, 88, 491–510.
26. Yang, L.Q.; Deng, J.; Wang, Z.L.; Guo, L.N.; Li, R.H.; Groves, D.I.; Danyushevsky, L.V.; Zhang, C.; Zheng, X.L.; Zhao, H. Relationships between gold and pyrite at the Xincheng gold deposit, Jiaodong Peninsula, China: implications for gold source and deposition in a brittle epizonal environment. *Economic Geology*. **2016b**, 111, 105–126.

27. Yang, L.Q.; Deng, J.; Li, R.P.; Guo, L.N.; Wang, Z.L.; Chen, B.H.; Wang, X.D. World-class Xincheng gold deposit: An example from the giant Jiaodong gold province. *Geoscience Frontiers*. **2016c**, 7, 419–430.
28. Groves, D.I.; Goldfarb, R.J.; Gebre-Mariam, M.; Hagemann, S.G.; Robert, F. Orogenic gold deposits: A proposed classification in the context of their crustal distribution and relationship to other gold deposit types.*Ore Geology Reviews*. **1998**, 13, 7–27.
29. Shepherd, T.J.; Rankin, A.H.; Alderton, D.H.M. *A practical guide to fluid inclusion dtudies*. Blackie: Chapman & Hall. **1985**, pp, 1–239.
30. Naden, J.; Shepherd, T.J. Role of methane and carbon dioxide in gold deposition. *Nature*. **1989**, 342, 793–795.
31. Brown, P.E. FLINCOR: a microcomputer program for the reduction and investigation of fluid-inclusion data. *American Mineralogist*. **1989**, 74, 1390–1393.
32. Roedder, E.; Bodnar, R.J. Geologic pressure determinations from fluid inclusion studies. *Annu. Rev. Earth Planet. Sci*. **1980**, 8, 263–301.
33. Xiong, Y.Q.; Shao, Y.J.; Zhou, H.D.; Wu, Q.H.; Liu, J.P.; Wei, H.T.; Zhao, R.C.; Cao, J.Y. Ore-forming mechanism of quartz-vein-type W-Sn deposits of the Xitian district in SE China: Implications from the trace element analysis of wolframite and investigation of fluid inclusions. *Ore Geology Reviews*. **2017**, 83, 152–173.
34. Van den Kerkhof, A.; Thiéry, R. Carbonic inclusions. *Lithos*. **2001**, 55, 49–68.
35. Taylor, H.P. The application of oxygen and hydrogen isotope studies to problems of hydrothermal alteration and ore deposition. *Economic Geology*. **1974**, 69, 843–883.
36. Hoefs, J. *Stable isotope geochemistry. sixth ed*. Springer Verlag, Berlin, Heidelberg. **2009**, pp, 130–135.
37. Hoefs, J. *Stable isotope geochemistry. third ed*. Springer-Verlag, Berlin Heidelberg. **1997**, pp, 1–201.
38. Schidowski, M.; Hayes, J.M.; Kaplan, I.R. Isotopic inferences of ancient biochemistry: carbon, sulfur, hydrogen and nitrogen. In: Schopf, J.W. (Ed.), Earth's Earliest Biosphere. *Princeton University Press, Princeton, NJ*. **1983**, pp, 149–186.
39. Faure, G. Principles of isotope geology. second ed. Wiley, New York, p. 589.*Geochronology Center Spec Publ*. **1986**, 4, 1–77.
40. Chen, H.Y.; Chen, Y.J.; Baker, M.J. Evolution of ore-forming fluids in the Sawayaerdun gold deposit in the Southwestern Chinese Tianshan metallogenic belt. *Journal of Asian Earth Sciences*. **2012**, 49, 131–144.
41. Ohmoto, H.; Rye, R.O. *Isotopes of sulfur and carbon In: Barnes, HL (Ed), Geochemistry of hydrothermal ore deposits, Second ed*. John Wiley and Sons, New York. **1979**, pp, 509–567.
42. Chaussidon, M.; Lorand, J.P. Sulphur isotope composition of orogenic spinel lherzolite massifs from Ariege (North-Eastern Pyrenees, France): An ion microprobe study. *Geochimica Et Cosmochimica Acta*. **1990**, 54, 2835–2846.
43. Zheng, Y.F.; Xu, B.L.; Zhou, G.T. Geochemical studies of stable isotopes in minerals. *Earth Science Frontiers*. **2000**, 7, 299–320. (in Chinese)
44. Deng, J.; Liu, X.F.; Wang, Q.F.; Pan, R.G. Origin of the Jiaodong-type Xinli gold deposit, Jiaodong peninsula, China: Constraints from fluid inclusion and C–D–O–S–Sr isotope compositions. Ore Geology Reviews. 2015, 65, 674-686.
45. Yang, L.Q., Deng, J.; Li, N.; Zhang, C.; Yu, J.Y. Isotopic characteristics of gold deposits in the Yangshan Gold Belt, West Qinling, central China: Implications for fluid and metal sources and ore genesis. Journal of Geochemical Exploration. 2016, 168, 103-118.
46. Ghebreab, W. Tectono-metamorphic history of Neoproterozoic rocks in eastern Eritrea. *Precambrian Research*. **1999**, 98, 83–105.
47. Albino, G.V.; Jalal, S.; Christensen, K. *Neoproterozoic mesothermal gold mineralization at Sukhaybarat East mine*. Transactions of the Institution of Mining and Metallurgy (Section B: Applied Earth Science). **1995**, 104, 157–170.
48. Walker, B.M.; Lewis, R.S.; Al Otaibi, R.; Ben Talib, M.; Christian, R.; Gabriel, B.R. *An Najadi gold prospect, Kingdom of Saudi Arabia; Geology and gold-resource assessment*. Saudi Arabian Deputy Ministry for Mineral Resources Technical Report, USGS-TR-94-5. **1994**, pp, 1-89.

49. Doebrich, J.L.; Zahony, S.G.; Leavitt, J.D.; Portacio Jr., J.S.; Siddiqui, A.A.; Wooden, J.L.; Fleck, R.J.; Stein, H.J. Ad Duwayhi, Saudi Arabia. Geology and geochronology of a Neoproterozoic intrusion-related gold system in the Arabian shield. *Economic Geology*. **2004**, 99, 713–741.
50. Billay, A.Y.; Kisters, A.F.M.; Meyer, F.M.; Schneider, J. The geology of the Lega Dembi gold deposit, southern Ethiopia: implications for Pan-African gold exploration. *Mineralium Deposita*. **1997**, 32, 491–504.
51. Andersson, U. B.; Ghebreab, W.; Teklay, M. Crustal evolution and metamorphism in east-central Eritrea, south-east Arabian-Nubian Shield. *Journal of African Earth Sciences*. **2006**, 44, 45–65.
52. Chen, Y.J.; Ni, P.; Fan, H.R.; Prajno, F.; Nai, Y.; Su, W.C.; Zhang, H. Diagnostic fluid inclusions of different types hydrothermal gold deposits. *Acta Petrologica Sinica*. **2007**, 23, 2085–2108. (in Chinese)
53. Goldfarb, R.J.; Groves, D.I. Orogenic gold: Common or evolving fluid and metal sources through time: *Lithos*. **2015**, 233, 2–26.